Conference on Modelling Fluid Flow (CMFF'25)
The 19th International Conference on Fluid Flow Technologies
Budapest, Hungary, August 26-August 29, 2025

NUMERICAL AND EXPERIMENTAL INVESTIGATION OF LOW REYNOLDS NUMBER FLOW IN A PACKED BED OF ROTATED BARS

Wojciech SADOWSKI[1,2], Christin VELTEN[3], Maximilian BRÖMMER[4], Hakan DEMIR[2], Francesca DI MARE[2], Katharina ZÄHRINGER[3], Viktor SCHERER[4]

[1] Corresponding Author, Email: wojciech.sadowski@rub.de
[2] Chair of Thermal Turbomachinery and Aero Engines, Ruhr University Bochum, UniversitätsstraSSe 150 D-44801 Bochum,
[3] The Laboratory of Fluid Dynamics and Technical Flows, Otto-von-Guericke-Universität Magdeburg.
[4] Institute of Energy Plant Technology, Ruhr University Bochum.

ABSTRACT

The present study focuses on the gas flow through an experiment-scale modular packed bed reactor consisting of square bars, arranged in layers. Each layer is rotated by 30^o resulting in a complex shape of the void spaces between the bars. Measurement results of the studied system are presented for particle-based Reynolds numbers $\mathrm{Re_p}$ of 100 and 200, and used as validation data for particle-resolved numerical simulations. The computations are performed for both $\mathrm{Re_p}$ using two different solid wall treatments: boundary conforming meshing and the blocked-off method. The flow inside the bed is largely independent of the Reynolds number and seems to be determined by the geometry of the void spaces. The flow in the freeboard is characterized by the presence of slowly dissipating jets downstream of the bed, which are characterized by unsteady oscillations for higher Reynolds number. The numerical results obtained with both boundary treatment approaches are in excellent agreement with the measurements inside the bed. In the freeboard, as a result of numerical properties of the current simulation approaches, some deviations between the simulation and measurements can be observed.

Keywords: packed bed, polyhedral particles, DNS, PIV, blocked-off method

NOMENCLATURE

$\mathrm{Re_p}$	$[-]$	particle Reynolds number
A	$[m^2]$	bed cross-section area
B	$[mm]$	bar size
Q	$[m^3/s]$	volumetric flow rate
T	$[s]$	time
$\langle w \rangle$	$[m/s]$	bulk velocity
u_ξ, w	$[m/s]$	velocity components
α	$[-]$	rotation angle
ϕ	$[-]$	porosity
ξ, z	$[m]$	coordinates

Subscripts and Superscripts

avg	averaging
i	initialization

1. INTRODUCTION

In packed-bed reactors, frequently used in chemical and process engineering, an assembly of particles is passed by a gas introducing reactants or facilitating processes, e.g., drying or coating. Hence, the flow characteristics (for example, dispersion of species, turbulence) influence the operation of packed-bed reactors to a large extent. At the same time, estimating these properties *a priori* is difficult, complicating design and leading to large error margins. A typical simplification in both analytical and numerical models is the assumption of spherical particles, which is often not appropriate when considering the randomly shaped polyhedra, or other industrially applied complex particle shapes [1]. At the same time, non-spherical geometry is known to influence the flow field to a large extent [2].

The use of Computational Fluid Dynamics (CFD) simulations, particularly the most accurate particle-resolved approach [3], can lead to valuable insight regarding the flow conditions, both in the packed beds and in the freeboard. The main drawback of the approach is its computational cost, resulting from the need to resolve the surface of each particle. Moreover, when a boundary conforming Finite Volume Method (FVM) is used, often a need to locally modify the geometry arises, to treat the regions of poor numerical stability near the contact points (surfaces) between individual particles [3].

Immersed boundary methods (IBM) are a common strategy to alleviate these issues, omitting the effort of boundary conforming mesh generation, treating contact points implicitly and avoiding expensive

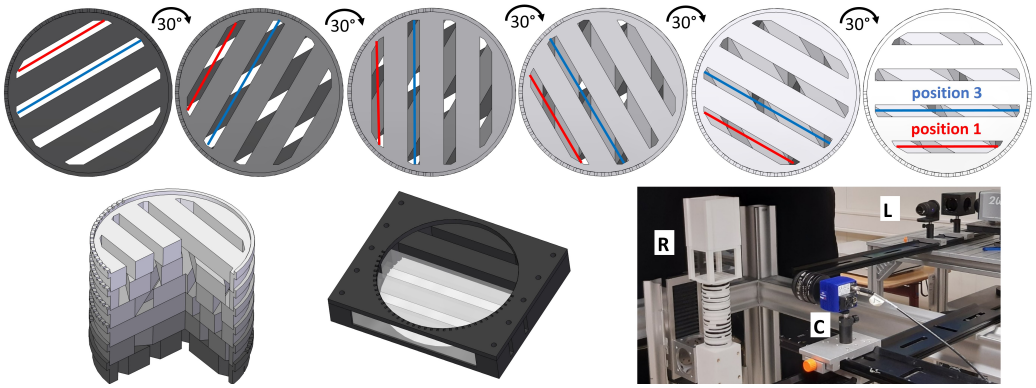

Figure 1. Schematic of the assembly process of a polyhedral packed bed assuming 30ř rotation between modules (upper line). The red and blue line mark the two measurement positions (P1 and P3) in different layers. The cut-out shows a complex structure of void spaces between the bars (lower left). To generate optical access an opaque standard module is replaced by a partially transparent optical module (lower centre). The PIV setup including the packed bed and measuring equipment is visible in the lower right part of the figure.

re-meshing in the case of moving objects. Numerous IBM approaches are available, among which the so-called *blocked-off method* introduced by Patankar [4] represents a simple variant of the method that does not involve complex interpolation schemes or surface reconstruction. It was recently validated against experimental measurements and smooth IBM for the simulations of packed beds [5]. Additionally, it was adopted to study the pressure drop over the bed of spherical particles [6] and used to construct a locally resolved flow model near the fuel lances of a reactor shaft [7]. A direct application of wall functions in case of higher Reynolds numbers and an easy integration into flow solvers are advantages of the present approach.

It is important to note that CFD-based predictions are of limited use without a proper validation using measurements of the flow properties, which are, however, rather scarce in packed bed reactors. Intrusive techniques Non-intrusive methods, which do not require optical access are typically limited to liquids [8] and their resolution is low compared to optical methods. For the latter, e.g., planar Particle Image Velocimetry (PIV) [9], the main difficulty lies in gaining an optical access to the interior of the packing. This is typically achieved via transparent packing material, which might require further post-processing.

Recently, Velten and Zähringer [10] used Particle Image Velocimetry (PIV) to measure both the flow in the interstices of a model packed bed with a BCC packing of spheres and the conditions above the bed. Although, the interstitial data was gathered only in a set of small, optically accessible regions, it enabled a detailed analysis of the flow field and validation of several methods and numerical codes [5, 11]. These applications highlight the synergies of combining experimental and numerical analyses for the study of flow conditions in packed beds.

Moving away from the typically assumed spherical particle geometry, in the present work, we investigate the flow in a packed bed, formed from the assembly of square bars. The configuration results in interstices with complex geometries with multiple inlets and outlets. The flow field is investigated experimentally, by the means of PIV, and numerically, by two different particle-resolved FVM-based simulation methods: the boundary-conforming, incompressible solver available in the OpenFOAM package and on the other side the blocked-off approach within the DEM/CFD framework of the Bulk-Reaction project also coupled with OpenFOAM. Two different Reynolds numbers are studied, and for each case, results are compared both within the bed and in the freeboard region.

2. PACKED BED GEOMETRY

The packed bed geometry is based on a modular design, in which each module consists of five parallel bars (square cross-section with size $B = 10\,mm$) spaced with a distance of $5\,mm$ inside dodecagon-shaped side walls. Additionally, the outer walls of the modules are circular (see fig. 1), allowing for each module to be rotated freely. This enables the study of various geometrical configurations at a constant porosity of $\phi = 0.332$, defined as a fraction of the void space volume to the volume of the module ($30\,cm^3$). In the current geometry, a total of 18 modules are combined, with the rotation angle of 30ř. This results in a bed height of $18B$, before the fluid enters into a rectangular outlet zone, where measurements are carried out above the bed. The flow is characterised by a particle Reynolds number based on bulk velocity $\langle w \rangle$ and the bar size $\mathrm{Re_p} = \rho \langle w \rangle B/\mu$. The velocity $\langle w \rangle$ is defined using the module cross-section area $A = 3000\,mm^2$ and the volumetric flow rate of the device $Q = A\phi\langle w \rangle$.

Table 1. Times used for collecting data in the experiments and each simulation: T_i start-up time, T_avg averaging time. The reference time scale is the flow through one module $T_B = B/\langle w \rangle$.

	exp.		b.-conf.		blocked-off
$\mathrm{Re_p}$	T_avg/T_B	T_i/T_B	T_avg/T_B	T_i/T_B	T_avg/T_B
100	755	12	88	75.5	226.5
200	1515	42	158	151.5	454.5

2.1. Experimental setup

To allow optical access inside the packed bed, a standard module is replaced by an optical one, where opaque bars are exchanged by transparent fused silica rods (fig. 1 lower center). The data has been gathered separately for the layers 15th to 17th and the freeboard region. For each module and the freeboard the data is gathered in two measurement planes (position 1 and 3, annotated with red and blue lines in fig. 1 and named P1 and P3 in the text), at the midspan of each void space between the bars. Flow data was averaged over 500 images, recorded with 10 Hz (50 s). In the current manuscript only the data from the 17th layer and the freeboard are discussed.

The full assembly of the packed-bed reactor (R) is presented in fig. 1 (lower right). Airflow is controlled by a Bronkhorst mass flow controller and seeded by Di-Ethyl-Hexyl-Sebacat (DEHS) tracer nebulized by a liquid nebulizer Type AGF 10.0 from Palas GmbH resulting in particle sizes below 10 μm. It enters into the packing through a diffuser filled with glass beads to homogenize the flow. The measurement region is illuminated by a double pulsed Quantel Q-smart Twins 850 Nd:YAG PIV-laser (L) and an Imager CX 12MP Camera (C) from LaVision GmbH records the PIV signal.

3. NUMERICAL MODEL

3.1. Simulations on the boundary-conforming mesh

The computations have been performed using OpenFOAM-12, using an unsteady solver, implementing the incompressible form of Navier–Stokes equations. The computational geometry is depicted in fig. 2. Based on the indications from our previous work, the flow conditions in the bed are influenced by the freeboard only in the topmost layers and are repeatable between layers [11]. Hence, to limit computational effort, only six top layers were realized in the simulation. The volume of fluid in the modules has been meshed with a boundary conforming hexahedral-dominant structured mesh (fig. 2). The initial mesh for the freeboard region has been generated in the same way, after which it was locally refined to allow for smooth transition in mesh resolution in both regions. The whole mesh, used for each simulation, consists of around 8.5M cells. The modules and the freeboard have been coupled using the Non-Conformal Coupling (NCC) interface. The uniform velocity profile with value $\langle w \rangle$ is prescribed at the inlet and the reference pressure value at the outlet. The rest of the boundaries are treated as no-slip walls.

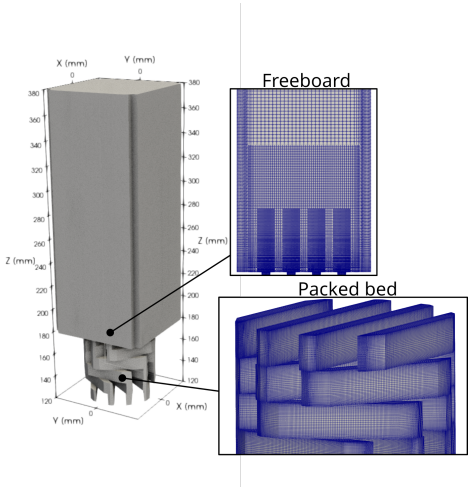

Figure 2. Domain used for the simulation with boundary-conforming mesh. Framed boxes illustrate the mesh used in the packed bed and the freeboard.

The time step of the simulation is adjusted to keep the Courant number under 0.6. Both spatial and temporal derivatives are computed using 2nd order schemes. PISO (Pressure-Implicit with Splitting of Operator) algorithm in the *consistent* variant is used to couple velocity and pressure, with 5 pressure corrector steps and 1 non-orthogonality correction step. To ensure that the flow is not influenced by initial conditions, sampling starts after an initial start-up time T_i which is presented along the sampling duration T_avg for all cases in table 1.

3.2. Simulations using the blocked-off method

The blocked-off method is based on creating an artificial boundary inside the computational grid. The current implementation is valid for particles of any shape and is described and validated in [5]. Flow variables in the cells obstructed by solid elements are set to the desired value which introduces a no-slip boundary condition at the solid-fluid interface. The original version by Patankar [4] involves the use of source terms. Here, we directly manipulate the coefficients in the system matrix to prevent complications in the calculation of residuals when solving the linear equation system. A general transport equation for a variable Φ, can be represented in algebraic form in any cell as $a_\mathrm{c}\Phi_\mathrm{C} + \sum_{N_\mathrm{c}} a_\mathrm{nb}\Phi_\mathrm{nb} = s_\Phi$, with a_c, a_nb and s_Φ denoting diagonal, non-diagonal matrix coefficients and source terms, respectively. Control volumes which are found to be in contact with a particle

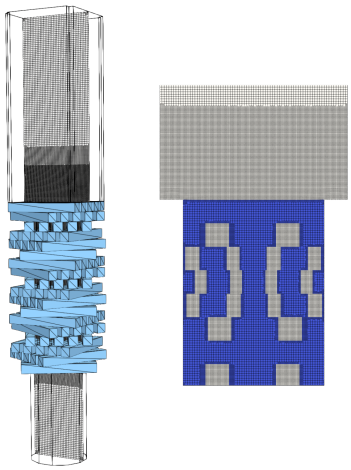

Figure 3. Particles and slice of mesh used in the blocked-off simulations. The right figure shows the mesh in the freeboard region with blocked fluid cells in blue.

are decoupled from the solution process by setting their non-diagonal contribution a_{nb} to zero and the diagonal coefficient a_{c} to one. Hence, inserting the desired value to the right-hand side results in specifying the cell value.

For the cells adjacent to these blocked volumes, the wall shear stresses are corrected to account for the case when particle faces are not aligned with the control volume faces. The stresses are estimated using tangential velocity and local distance from the particle surface, and used in a source term that replaces the viscous contribution at the solid-fluid interface in the momentum equation. Additionally, the Neumann boundary condition in the pressure equation at the solid-fluid interface is enforced by setting the matrix coefficient a_{nb} to a very low value.

The simulations using the blocked-off method are realized with the Bulk-Reaction DEM/CFD framework where a finite volume fluid solver based on *fireFoam* (OpenFOAM v2012) is utilized. The bars in the test rig are represented by cuboid particles which influence the fluid flow via the blocked-off methodology. Total of 90 cuboid particles are generated according to the bar dimensions and placed in the domain as in fig. 3. For the fluid flow computation, a cartesian grid fitted to the experimental rig is created. The dodecagon shape of the walls at the particle bed section is extended for the inlet. Mesh refinement is applied in the void spaces as well as up- and downstream of the particle region. In relation to the particle width, particles are discretised by $B/\Delta x = 20$ leading to a total number of 5.1M cells. The same mesh is used for all Reynolds numbers. The Courant number is kept between values of 0.1-0.3. The PISO algorithm is utilized to solve the evolution of the flow field with one non-orthogonal corrector step to account for the polyhedral cells at the walls of the test rig. In general, 2nd order schemes are applied in the discretisation of the transport equations, while for convection a 2nd order upwind scheme is employed to prevent pressure oscillations. Sampling times for averaging are reported in table 1.

4. RESULTS

4.1. Flow inside the bed

The flow inside the packed bed is visualised in detail in the figs. 4 and 5. In each of the figures, a coordinate system defined on the measurement plane is used, with ξ denoting the horizontal coordinate. Moreover, only the velocity components tangent to the measurement plane are plotted: w is the vertical velocity and u_ξ is the horizontal velocity along the measurement plane.

The velocity field is mainly determined by the adopted geometry and the connectivity between the void spaces in the layers. The P1 (position 1, see fig. 1) interstices have two inlets and two outlets, in a staggered arrangement due to the rotation of the module. The P3 interstice (position 3, see fig. 1) on the other hand have three inlets/outlets. In both P1 and P3 slits, the fluid is accelerated in the inlet and its further behaviour is determined by the positions of the outlets. In case of P1, the flow impinges on the top wall of the module and is forced to split into two outlets. This results in most of the flow converging from both inlets into the right outlet, while the rest is redirected into the left outlet, which has also a much smaller cross-section area. Inside P3, the outlets are much more closely aligned with the inlets, hence, a strong upwards flow can be observed. The regions positioned between the inlet/outlet pairs are characterised by a lateral flow, presumably driven by the pressure difference between these areas. This behaviour leads to the presence of recirculation regions, attached to the left side of the in-flowing streams.

Overall, the simulation results agree very well with the PIV measurements. The main differences can be observed in the far left and right areas of the measured regions. For example, for both Re, based on streamline visualisation, the PIV data indicates fluid crossing the boundary of the measured region on the left side of P1 and P3. This effect is observed due to the necessary modification of the geometry to enable the optical access to the interstices, which creates additional space on the left and right side (a standard module has a solid wall at these positions). Interestingly, this "outflow" is much stronger in P1 than P3, where the flow is directed more upwards near the left and right boundaries of the measurement region. It is probable that the impact of the modification of the geometry on the measured results is stronger in slits with stronger lateral flow.

On the other hand, simulation data suggests that the presence of the wall results in recirculation regions attached to the bottom left and top right corners of P1 region. The differences in the flow field

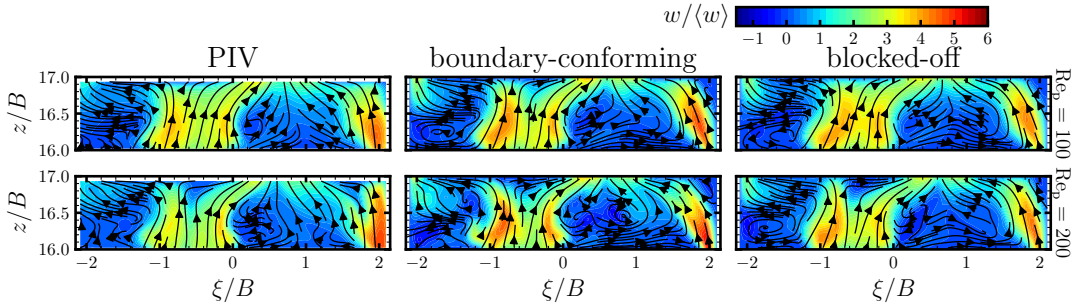

Figure 4. Velocity field at the measurement position 1 inside layer 17, visualised using streamlines. Color denotes the vertical component $w/\langle w\rangle$. Plotted data has been gathered using PIV and simulation approaches: boundary-conforming and blocked-off methods, at $\mathrm{Re_p} = 100$ (top) and 200 (bottom).

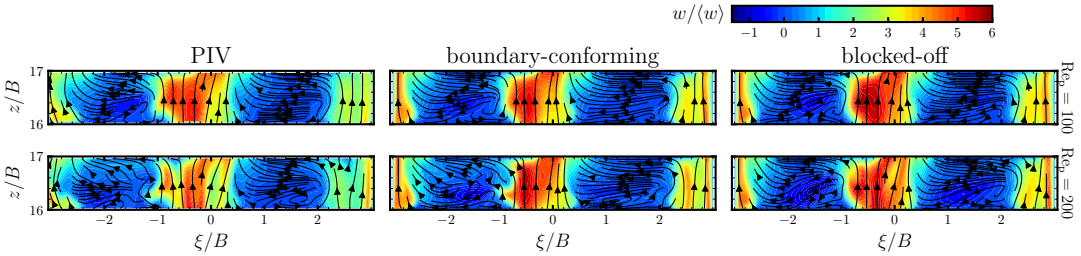

Figure 5. Velocity field at the measurement position 3 inside layer 17, visualised using streamlines. Colormap denotes the vertical component $w/\langle w\rangle$. Plotted data has been gathered using PIV and simulation approaches: boundary-conforming and blocked-off methods, at $\mathrm{Re_p} = 100$ (top) and 200 (bottom).

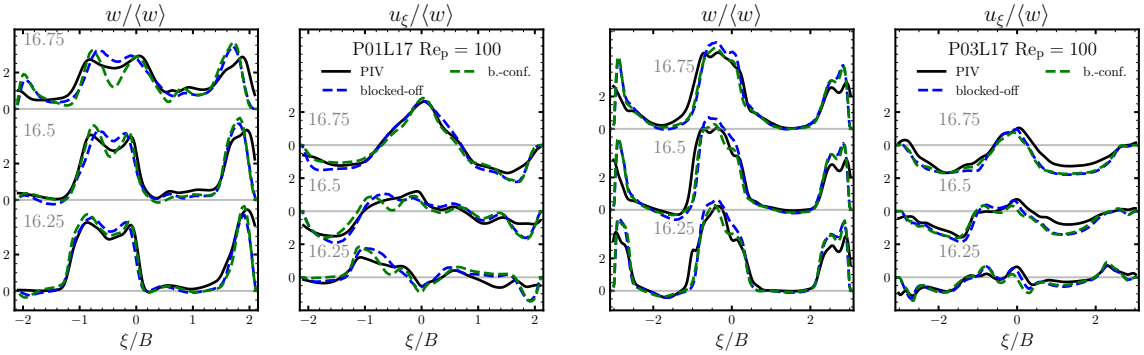

Figure 6. Velocity inside the bed for $\mathrm{Re_p} = 100$, plotted along the lines defined in planes P1 (left) and P3 (right) in the 17th layer. The gray numbers correspond to z/B coordinate.

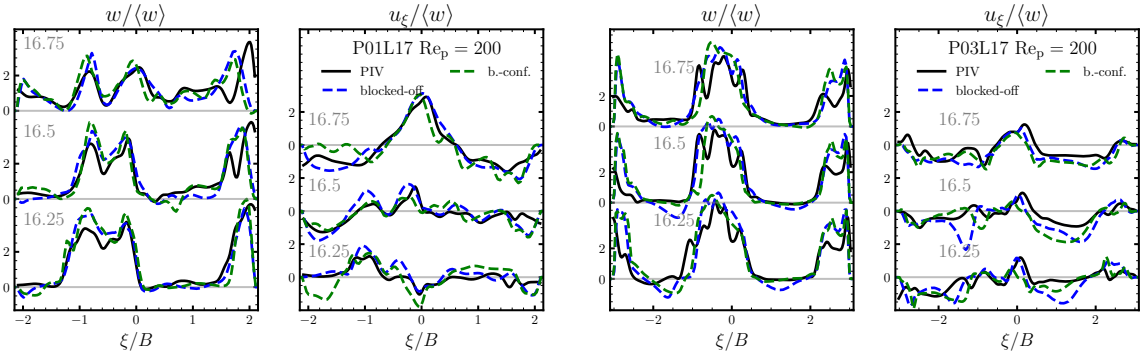

Figure 7. Velocity inside the bed for $\mathrm{Re_p} = 200$, plotted along the lines defined in planes P1 (left) and P3 (right) in the 17th layer. The gray numbers correspond to z/B coordinate.

near the side walls, can be observed in figs. 6 and 7. Both simulation approaches predict a different shape of boundary layer jets (P1 for large ξ and P3 for both sides of measurement region), with the simulations consistently overpredicting the maximum streamwise velocity in these regions. At the larger Reynolds number the differences between the measured and simulated flow fields grow larger. The differences between the numerical representations and real experimental setup have strong influence on the resulting flow field.

Although, the flow fields are largely similar across the two Reynolds numbers, the increase in the fluid's inertia influences the shapes and sizes of the separated flow regions. At P1, the increase of Reynolds number leads to a much more complex flow field between the two inlets, with recirculating flow appearing in the middle of the measurement section. At the other position, larger $\mathrm{Re_p}$ leads to increased separation on the right side of the measured region. On the left side, however, it seems that a faster reattachment can be observed. PIV data also indicates that the non-uniformity of the flow field is much stronger at larger $\mathrm{Re_p}$, although this effect is not fully represented in the simulation data.

Though the boundary-conforming and blocked-off approach yield different mesh refinements close to walls/particles (typical near-wall boundary layer refinement vs. equally spaced mesh), the line plots in figs. 6 and 7 show almost no difference in the prediction of the wall jets for $\mathrm{Re_p} = 100$ and slight differences for larger $\mathrm{Re_p}$. Especially in comparison to the deviation between simulations and experiment, these are negligible. Based on these results, the handling of the wall flow with the blocked-off approach seems to be appropriate for these Reynolds numbers. In general, the numerical methods align very well in the void space with only minor differences in height and shape of the jets. The strongest difference between the two simulation approaches are found for horizontal component u_ξ with $\mathrm{Re_p} = 200$ at P1 where a more pronounced horizontal motion in the recirculation region is predicted by the boundary-conforming method in contrast to the blocked-off approach and the experiment.

4.2. Freeboard

The flow field in the freeboard is visualised in fig. 8. It is dominated by jets issuing directly from the outlets of the last module. Hence, there are two and three jets present on planes P1 and P3, respectively. The resulting velocity field is quite complex with several recirculation regions present in between the jets and the walls of the model packed bed.

At lower $\mathrm{Re_p}$, in the P1 plane, the jets combine relatively quickly above the bed surface. At the sides of the measured region, the air is sucked into the freeboard from the outlet with relatively slow velocity, forming two large recirculation regions near the walls of the channel. As the Reynolds number increases, the momentum of the jets is redistributed laterally quicker by low-velocity vortical motions, resulting in a more uniform velocity in the middle of the outlet region. The interaction between both streams also results in a swirling flow between them, and smaller recirculation regions above the bed surface.

In the P3 plane, the effect of backflow into the freeboard from the outlet is much weaker, even at the lower Reynolds number. The leftmost jet impinges onto the downward moving air and is redirected, first, towards the bed surface, and into the middle jet. This phenomenon impacts the momentum distribution above the bed, and it could influence the scalar mixing in such systems as it reintroduces the gas which already left the reactor back into the bed. The increase of the inertial effects leads to more pronounced jets and, although, the left jet dissipates quicker then the other ones, much less of the ejected fluid is redirected into the middle one. Additionally, the unsteadiness at larger $\mathrm{Re_p}$ results in more diffusive behaviour of the jet downstream.

In general, a good agreement could be reached by the three methods especially for the low $\mathrm{Re_p}$ case. Figure 9 shows that the agreement is best in close distance to the bed surface. While excellent agreement of the boundary-conforming method is reached at $z/B = 19$, the blocked-off method predicts a too narrow jet on the left in P1 and a slight overshoot of the centre jet in P3 for the vertical velocity w, which also leads to a bigger discrepancy in the horizontal velocity component u_ξ.

As the distance from the bed surface increases, differences between simulations and the experiment get more pronounced. Here, the 3D interaction of the jets comes into play, causing small discrepancies in the jets to accumulate to larger deviations from experimental data. The errors in momentum prediction are probably caused by a limited resolution downstream of the bed surface diffusing and dampening the breakdown of the jets into smaller vortical structures. Alternatively, different conditions at the domain outlet (fixed pressure condition for simulations vs. small environmental interference in the experiment) may also contribute to different velocity fields above the bed.

Following the line plots of the higher Reynolds number in fig. 10, the agreement of the numerical data with the PIV data is again best close to the bed surface for P1. In the experiment and the blocked-off simulation the mean jets dissipate faster than in the body-conforming case. For P3, the outer jets are reproduced well but the centre jet shows a different flow structure with two velocity peaks in the numerical data for $z/B = 19$ and 21. Importantly, the accuracy of the simulation data might be limited by a relatively short averaging time (especially in case of the boundary-conforming method). Previous work [11] indicated that in such systems, exceedingly long averaging times are required to fully capture the dynamics of the freeboard. Although, the convergence

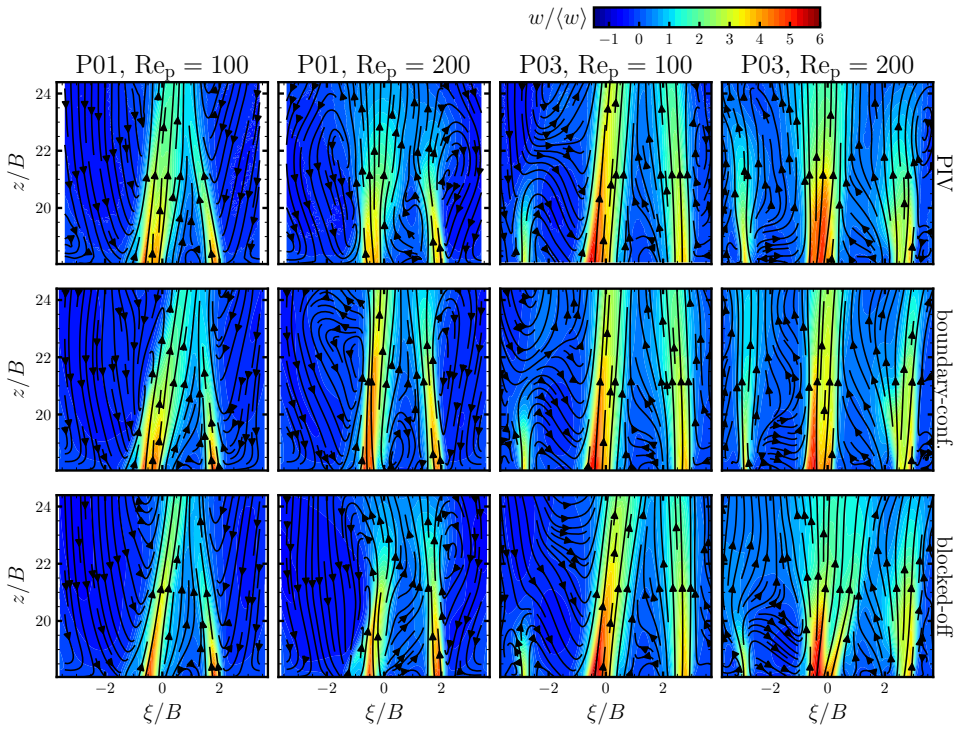

Figure 8. Velocity in the freeboard for $\mathrm{Re_p} = 100$, plotted along the lines defined in planes P1 (left) and P3 (right). The gray numbers correspond to z/B coordinate.

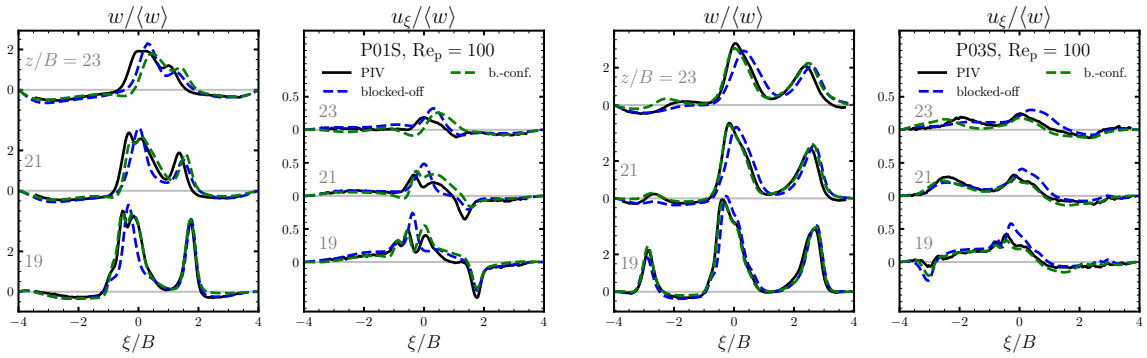

Figure 9. Velocity in the freeboard for $\mathrm{Re_p} = 100$, plotted along the lines defined in planes P1 (left) and P3 (right). The gray numbers correspond to z/B coordinate.

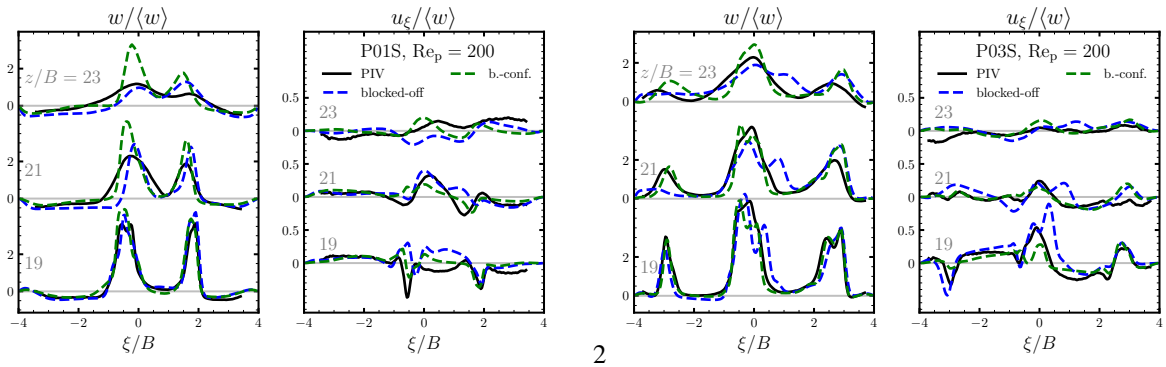

Figure 10. Velocity in the freeboard for $\mathrm{Re_p} = 200$, plotted along the lines defined in planes P1 (left) and P3 (right). The gray numbers correspond to z/B coordinate.

of statistics has to be further assessed the overall nature of the flow field is reproduced correctly by both simulation approaches.

5. CONCLUSIONS & OUTLOOK

In this contribution, the flow through a modular packed bed of bar-like particles and in the freeboard is examined by PIV measurements, and by conducting simulations with a boundary-conforming and a blocked-off approach. Two different Reynolds numbers are considered, Re_p = 100 and 200.

The flow inside the packed bed reveals good agreement between the experiment and simulations. Differences are majorly found due to geometry adjustments needed to measure the flow field between the particles. The increase of Reynolds number only slightly affects the flow features in the void spaces, which are determined to a large extent from the geometry and alignment of inlets/outlets in each interstice. While the simulation approaches do not show significant differences inside the bed, stronger deviations are found in the flow at the freeboard. The boundary-conforming simulations agree very well with experiments right at the bed surface while different rate of the dissipation of the jets issued into the freebord can be observed. Better agreement is found in the blocked-off cases but mismatches between the emerging jets are still visible, potentially due to an insufficient mesh refinement in the freeboard.

The blocked-off method has been found to capture adequately all flow features inside the bed, while allowing for minimisation of required mesh size and computational effort. The Non-Conformal Coupling interfaces coupling the modules in boundary conforming mesh, have resulted in stable and accurate solution, enabling the future studies of non-static packed beds with rotating modules. Further investigations of the current case are needed to fully assess the accuracy of the simulation approaches, concentrating on the fluctuations in the freeboard, the corresponding turbulent kinetic energy, and the influence of the averaging time on the results. Furthermore, higher Reynolds number cases would be of interest to get more knowledge about industrial packed beds' conditions.

ACKNOWLEDGEMENTS

This work was funded by the Deutsche Forschungsgemeinschaft (DFG, German Research Foundation) Project-ID 422037413 - TRR 287 and project number 279416000.

REFERENCES

[1] Rosseau, L. R., Middelkoop, V., Willemsen, H. A., Roghair, I., and van Sint Annaland, M., 2022, "Review on Additive Manufacturing of Catalysts and Sorbents and the Potential for Process Intensification", *Frontiers in Chemical Engineering*, Vol. 4.

[2] Moghaddam, E., Foumeny, E., Stankiewicz, A., and Padding, J., 2019, "Fixed bed reactors of non-spherical pellets: Importance of heterogeneities and inadequacy of azimuthal averaging", *Chemical Engineering Science: X*, Vol. 1, p. 100006.

[3] Jurtz, N., Kraume, M., and Wehinger, G. D., 2019, "Advances in Fixed-Bed Reactor Modeling Using Particle-Resolved Computational Fluid Dynamics (CFD)", *Reviews in Chemical Engineering*, Vol. 35 (2), pp. 139–190.

[4] Patankar, S., 1980, *Numerical Heat Transfer and Fluid Flow*, Hemisphere Publishing Company.

[5] Gorges, C., Brömmer, M., Velten, C., Wirtz, S., Mahiques, E. I., Scherer, V., Zähringer, K., and van Wachem, B., 2024, "Comparing two IBM implementations for the simulation of uniform packed beds", *Particuology*, Vol. 86, pp. 1–12.

[6] Brömmer, M., Scharnowski, M., Illana Mahiques, E., Wirtz, S., and Scherer, V., 2024, "Investigating the inflow into a granular bed using a locally resolved method", *Particuology*, Vol. 85, pp. 89–101.

[7] Illana Mahiques, E., Brömmer, M., Wirtz, S., and Scherer, V., 2023, "Locally Resolved Simulation of Gas Mixing and Combustion Inside Static and Moving Particle Assemblies", *Chemical Engineering & Technology*, p. ceat.202200622.

[8] Lovreglio, P., Das, S., Buist, K. A., Peters, E. A. J. F., Pel, L., and Kuipers, J. A. M., 2018, "Experimental and numerical investigation of structure and hydrodynamics in packed beds of spherical particles", *AIChE Journal*, Vol. 64 (5), pp. 1896–1907.

[9] Khayamyan, S., Lundström, T. S., Gren, P., Lycksam, H., and Hellström, J. G. I., 2017, "Transitional and Turbulent Flow in a Bed of Spheres as Measured with Stereoscopic Particle Image Velocimetry", *Transport in Porous Media*, Vol. 117 (1), pp. 45–67.

[10] Velten, C., and Zähringer, K., 2023, "Flow Field Characterisation of Gaseous Flow in a Packed Bed by Particle Image Velocimetry", *Transport in Porous Media*, Vol. 150, pp. 307–326.

[11] Sadowski, W., Sayyari, M., Di Mare, F., Velten, C., and Zähringer, K., 2024, "Particle-Resolved Simulations and Measurements of the Flow through a Uniform Packed Bed", *Physics of Fluids*, Vol. 36 (2), p. 023330.